Nuclear Instruments and Methods in Physics Research B 306 (2013) 265–270

Contents lists available at SciVerse ScienceDirect

Nuclear Instruments and Methods in Physics Research B

journal homepage: www.elsevier.com/locate/nimb

Improved beam spot measurements in the 2nd generation proton beam writing system

Yong Yao [a], Martin W. van Mourik [b], P. Santhana Raman [a], Jeroen A. van Kan [a,*]

[a] Centre for Ion Beam Applications, Department of Physics, National University of Singapore, Singapore 117542, Singapore
[b] Coherence and Quantum Technology, Department of Applied Physics, Eindhoven University of Technology, 5600 MB Eindhoven, The Netherlands

ARTICLE INFO

Article history:
Received 9 August 2012
Received in revised form 16 October 2012
Available online 10 November 2012

ABSTRACT

Nanosized ion beams (especially proton and helium) play a pivotal role in the field of ion beam lithography and ion beam analysis. Proton beam writing has shown lithographic details down to the 20 nm level, limited by the proton beam spot size. Introducing a smaller spot size will allow smaller lithographic features. Smaller probe sizes, will also drastically improve the spatial resolution for ion beam analysis techniques. Among many other requirements, having an ideal resolution standard, used for beam focusing and a reliable focusing method, is an important pre-requisite for sub-10 nm beam spot focusing. In this paper we present the fabrication processes of a free-standing resolution standard with reduced side-wall projection and high side-wall verticality. The resulting grid is orthogonal (90.0° ± 0.1), has smooth edges with better than 6 nm side-wall projection. The new resolution standard has been used in focusing a 2 MeV H_2^+ beam in the 2nd generation PBW system at Center for Ion Beam Applications, NUS. The beam size has been characterized using on- and off-axis scanning transmission ion microscopy (STIM) and ion induced secondary electron detection, carried out with a newly installed micro channel plate electron detector. The latter has been shown to be a realistic alternative to STIM measurements, as the drawback of PIN diode detector damage is alleviated. With these improvements we show reproducible beam focusing down to 14 nm.

1. Introduction

To overcome the diffraction constraints of traditional optical lithography, the next generation lithographies (NGLs) will utilize any one or more of EUV (extreme ultraviolet), X-ray, electron or ion beam technologies to produce sub-100 nm features. Proton beam writing (PBW), as an ion beam technique, has flexibility and potential to become leading contender as NGL [1]. In PBW system, a high energy (~MeV) proton beam from an ion accelerator is focused down to sub-100 nm using magnetic quadrupole lenses. Then this highly focused proton beam is scanned over a pre-defined area on a resist coated sample to form high aspect ratio 3D nanostructures [2,3]. In addition to PBW, nano-sized proton beams are also used as a probe for various ion beam analysis techniques, such as particle induced X-ray emission, Rutherford backscattering spectrometry, ion beam induced charge [4]. Achieving smaller probe size will directly result in improving the spatial resolution of the above mentioned techniques.

Initially, commercial resolution standards were used in PBW experiments to focus the proton beam to sub-micron regimes. At the point that sub-100 nm beam focusing had become possible, these commercial resolution standards with improper edge definition and rough surface became futile. Thus, a resolution standard with better side-wall verticality and side-wall smoothness needed to be fabricated, so as to be used in the sub-100 nm beam focusing experiments [5,6]. PBW has demonstrated high aspect ratio 3D micro/nano-structure fabrication with precise edges, smooth and straight side-walls due to its reduced proximity effects [7]. Recently, 2 μm thick free standing Ni resolution standards with superior characteristics, fabricated using PBW technique, were found to be more useful than the commercial grids for focusing to sub-30 nm beam spot sizes [5]. These were reported to have smooth and straight side-walls, with a side-wall verticality of 89.4° and an average side-wall projection to the beam of around 20 nm. Presently, with the 2nd generation [8] PBW facility commissioned at Center for Ion Beam Applications (CIBA), National University of Singapore, it is possible to obtain sub-20 nm beam spot sizes for PBW experiments [9]. Since reaching sub-20 nm beam spot sizes, these resolution standards have become inaccurate in determining the lower limit of proton beam focusing. This handicapped situation motivates us to fabricate a free-standing Ni resolution standard with high degree of orthogonality, smoothness, improved side-wall verticality and reduced side-wall projection, using the 2nd generation PBW system.

* Corresponding author.
E-mail address: phyjavk@nus.edu.sg (J.A. van Kan).

0168-583X/$ - see front matter © 2012 Elsevier B.V. All rights reserved.
http://dx.doi.org/10.1016/j.nimb.2012.10.033

A second requirement for accurate beam focusing is the introduction of a reliable method of imaging the proton probe size. Primarily, ion detection and secondary electron detection are commonly used techniques to characterize the probe beam [10,11]. Ion detection is done using both off-axis and on-axis scanning transmission ion microscopy (STIM). In secondary electron detection method, the secondary electrons are detected with an annular micro-channel plate (MCP). Since beam characterization using secondary electron detection has a few inherent advantages like high detection sensitivity (when compared with off-axis STIM), prolonged life-time of the detector, and enhanced imaging quality, we have installed an annular MCP in the 2nd generation PBW endstation.

In this paper we present the fabrication processes and characterization of orthogonal free standing Ni resolution standards, potentially capable of measuring sub-10 nm beam spot sizes. Secondly, we compare different detection methods (STIM and secondary electron detection method) used in focusing a high energy ion beam, using the new resolution standard.

2. Experimental procedures

2.1. Fabrication of free-standing Ni resolution standard

Poly-methyl methacrylate (PMMA) has exhibited sub-100 nm features and extremely smooth sidewalls (2–3 nm root mean square) when exposed by proton beam [12]. Therefore we have decided to use PMMA as a mold to fabricate a free standing fine Ni grid. Results from SRIM [13] simulations, performed for a parallel 2 MeV proton beam passing through 1.5 μm PMMA, show that the beam spread in the region between 1 and 1.5 μm in PMMA (where ~500 nm thick Ni will be electroplated for fine grid) is less than 3 nm or a sidewall slope of 89.7°. The fabricated fine free-standing Ni grid area is supported by a 20 μm thick Ni grid. AR-p 3210 (ALLRESIST) is a positive resist under UV exposure; this AR-p is a suitable candidate for thick layers in combination with Ni plating and resist removal.

The fabrication of our free-standing resolution standard has multiple steps: (1) preparation of the PMMA layer, (2) PBW and Ni electroplating for fine grid, (3) preparation of 20 μm thick support grid and (4) releasing free-standing resolution standard from the substrate. These steps are explained schematically in Fig. 1 and are also briefly described;

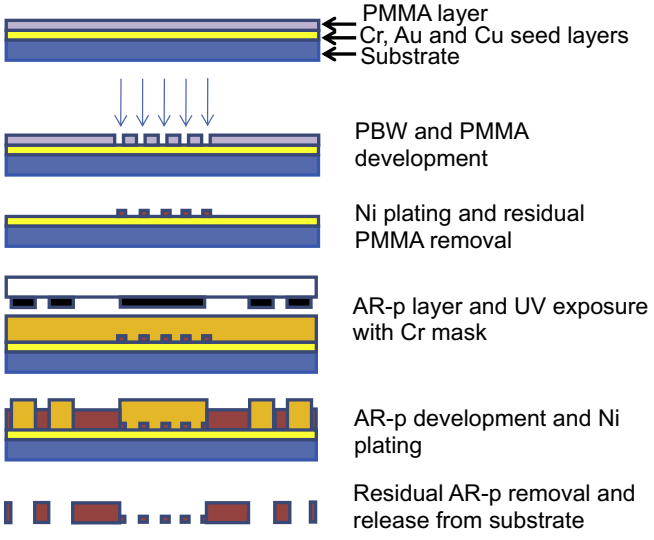

Fig. 1. Schematic representation of free-standing Ni grid fabrication processes.

Step (1): *Preparation of the PMMA layer:* A silicon wafer was first sputtered with a thin layer of Cr (20 nm), Au (200 nm) and Cu (100 nm). The Cr layer was added to enhance the adhesion of the Au layer to the Si substrate. The Au and Cu layers have good conductivities and will act as seed layers for the electroplating. The Cu layer can also be easily etched without damaging the later electroplated Ni layer. Then, a 2 μm PMMA (PMMA-A11 from Microchem) layer was spin coated on the sample.

Step (2): *PBW and Ni electroplating for fine grid:* A 2 MeV proton beam with a beam spot size of about $400 \times 400\ nm^2$ was used in this PBW experiment. A fine grid (total area of $300 \times 300\ \mu m^2$) was written on PMMA by exposing it to the proton beam through stage plus beam scanning method (stage scanning velocity: 2 μm/s, beam scan width 5 μm). After exposing the sample to a fluence of $\sim 200\ nC/mm^2$, it was developed using Isopropyl alcohol and DI water (7:3 by volume) for 2.5 min followed by a DI water rinse [5]. Then, a 500 nm Ni layer was electroplated and the residual PMMA was then removed by toluene at a temperature of 45 °C for 90 min.

Step (3): *Preparation of 20 μm thick support grid:* A 30 μm thick AR-p layer was spin coated on the sample and UV lithography (365 nm) through a Cr mask was used to create $250 \times 250\ \mu m^2$ squares well aligned with the plated fine Ni grid. The AR-p was then developed by AR 300-26. Subsequently, a 20 μm Ni layer was electroplated and the residual AR-p was removed.

Step (4): *Releasing free-standing resolution standard:* The Cu sacrificial layer was etched in a sodium persulfate solution at 45 °C [14]. After about 20 min, the free standing resolution standard was released and characterized. Later it was mounted onto the sample stage for beam focusing experiments.

2.2. Installation of secondary electron detector

In the 2nd generation PBW line, until now the beam diagnostics has been carried out through ion detection method using both on and off-axis STIM technique. A PIN diode detector (Make: Hamamatsu, Model: S1223), with an active detection area of $6.6\ mm^2$, is positioned behind the sample on a linear translator. When an incoming beam is scanned over an area on the resolution standard, the direct (un-scattered) beam passing through the Ni grid is energy selected during on-axis STIM measurements, whereas the scattered beam is analyzed in off-axis STIM mode. PIN diodes have inherent problems of detector damage within a short duration of beam exposure, possibly resulting in inaccurate beam diagnostics. Alternatively, beam characterization can be accomplished using secondary electron detection. When a fast moving ion penetrates a substrate, its dominant energy loss would be due to ion–electron interaction. During such collisions the substrate electrons are set to either excite or eject from their orbit (called secondary electrons) [15]. Such secondary electrons having enough energy to overcome the surface barrier potential of the substrate are detected by an annular electron detector (Manufacturer: NVT, Model: NVT2C45/C4M10) [16], placed 8 mm upstream with respect to the sample plane. A schematic overview of the set-up is shown in Fig. 2. Earlier in the 1st generation PBW beam line, electron detection has been carried out successfully using single channel electron multipliers (CEMs) [10]. The MCP detector has a higher yield compared to CEMs used by CIBA, due to the larger solid angle, resulting in a five-fold increase in sensitivity compared to the 1st generation PBW line. Details on beam focusing procedure can be found in Ref. [17].

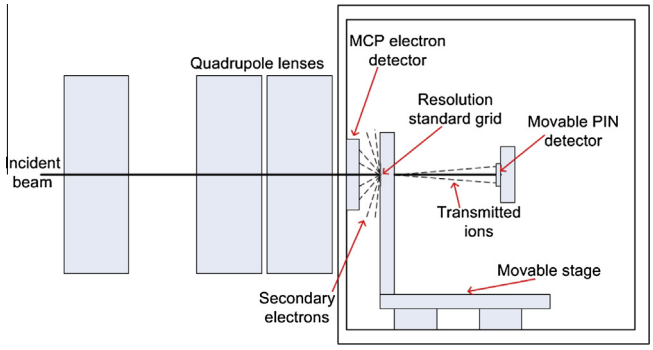

Fig. 2. Schematic of 2nd generation PBW end-station. An incident ion beam passes through a series of quadrupole magnetic lenses, focusing it in both transverse directions onto a resolution standard grid. The grid is placed in a holder on a movable stage. Secondary electrons and transmitted ions are detected by an MCP electron detector and movable PIN detector, respectively.

3. Characterization

Fig. 3 shows optical micrographs (Fig. 3a and b) and secondary electron microscopy (SEM) images (Fig. 3c and d) of the new free-standing resolution standard from the front side, which was originally attached to the Cu layer. From these images it is evident that the vertical and horizontal Ni grids are highly orthogonal ($90.0° \pm 0.1$) to each other. On analyzing multiple SEM images (including Fig. 3d) the free-standing resolution standard, is generally found to have smooth surfaces. Furthermore, from SEM images (not shown here) it has been confirmed that the grid is about 500 nm thick with a sidewall slope projection of less than 5–6 nm. The inaccuracy of the sidewall slope projection is due to the limited quality of the SEM images.

This newly fabricated free-standing resolution standard was used to focus a 2 MeV H_2^+ ion beam. Initially the incoming ion beam passes through object slits of $6 \times 2\ \mu m^2$ opening, further collimated by aperture slits of $10 \times 10\ \mu m^2$. The ion beam is then focused onto the resolution standard by a set of magnetic quadrupole lenses (used in spaced triplet configuration). A count rate of about 20,000 protons per second has been recorded using on-axis STIM.

The beam focusing was monitored by using a combination of secondary electron detection, off- and on-axis STIM measurements. The beam was scanned over the Ni resolution standard. The beam has been focused down to a spot size of $14 \times 39\ nm^2$ at FWHM, as calculated from the beam profile acquired using on-axis STIM. After having been focused (initially using on-axis STIM, Fig. 4a), different detection methods were used to investigate their imaging quality, as shown in Fig. 4b (off-axis STIM) and Fig. 4c (MCP image). These images were recorded using the same beam parameters with a scan size of $2.72 \times 2.72\ \mu m^2$ and a scan digitization of 512×512 pixels. We observed a reduced count rate on STIM images due to the PIN diode detector damage caused by the irradiation of high beam intensity per unit area, as reported earlier by Minqin et al. [11]. When measuring beam profiles the beam is scanned over a single line repeatedly as indicated in Fig. 4a and c, causing local detector damage at a faster rate [11]. Whereas the count rate of secondary electrons, measured by the MCP, remained constant throughout the entire experiment. More-

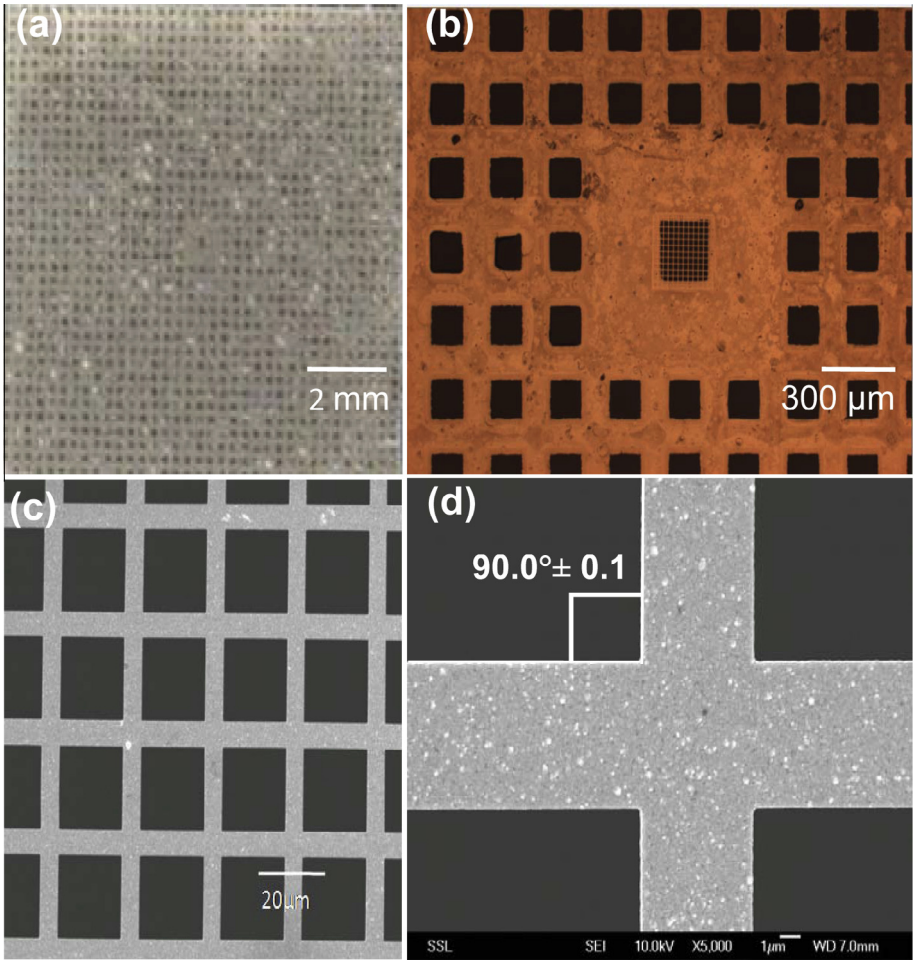

Fig. 3. (a and b) Optical micrographs and (c and d) SEM images of the final free-standing Ni resolution standard grid.

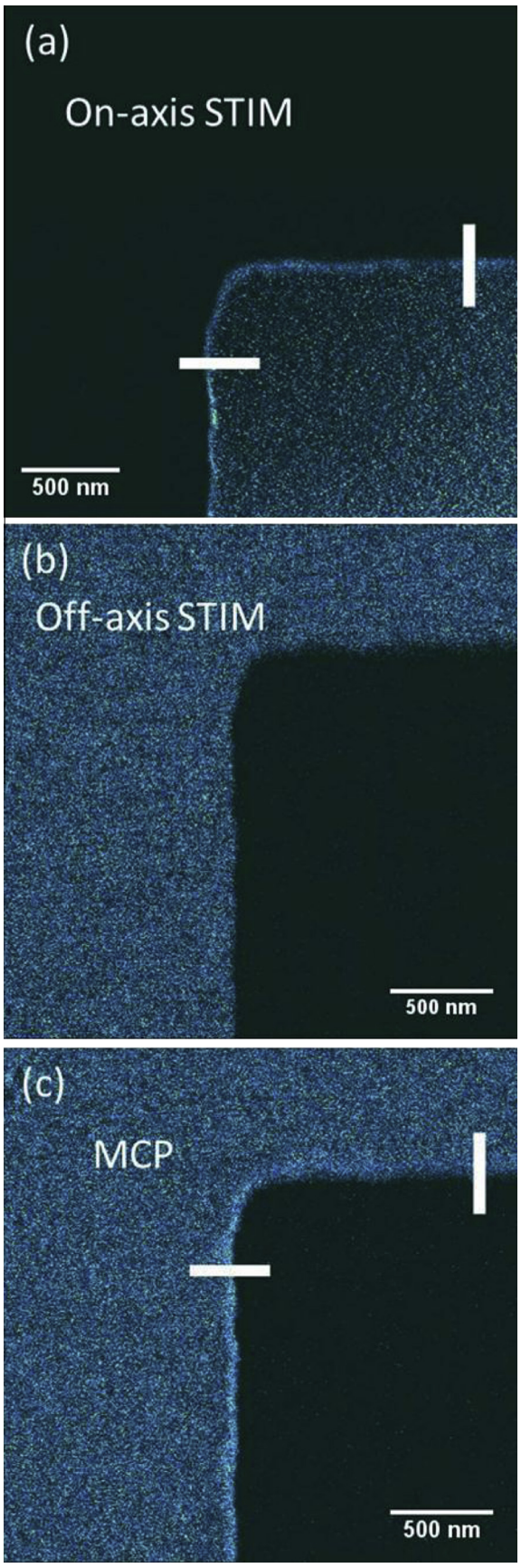

Fig. 4. Images of a 500 nm Ni grid obtained through on- and off-axis STIM measurements using a PIN diode detector (a and b), and MCP detector (c).

over, the yield of secondary electrons, as recorded by the MCP detector, is about 5–6 electrons per 10 protons, which is a drastic improvement over the 1/10 e/p in the 1st generation PBW line. The fact that the MCP detector yield does not deteriorate during experiments makes electron detection a more suitable and reliable technique for longer measurements. In the case of PBW, the typical current required for lithography is about 1000 times larger than what has been used in these focusing experiments, beam currents at these rates, for on-axis STIM measurements, would destroy the PIN detector in seconds.

Fig. 5 shows the beam profile measurement carried out by repeatedly scanning over a single line in the x and y direction, over the edge of the grid (from the region as shown with a white marker line in Fig. 4a and c). The results have been fitted using a model for secondary electron scattering as described by Udalagama et al. [18], where the profile as a function of position X_0 is given by

$$F(X_0, f, a) = H_{err}\left[1 + erf\left(\frac{2\sqrt{\ln(2)}}{f}(a - X_0)\right)\right] + H_{gau}\left[\exp\left(-\frac{\ln(16)}{f^2}(a - X_0)^2\right)\right]$$

where f is the beam's FWHM and a is the position of the grid's edge. The term containing the factor H_{err} is the output due to the beam being scanned over an ideal edge, and the term containing H_{gau} is the distortion of the output due to edge enhancement. The term H_{gau} has been set to zero for STIM measurements, and in MCP measurements where there was no visible edge enhancement. Using on-axis STIM and electron detection, a beam size of $14 \times 39\ nm^2$ (Fig. 5a and b) and $31 \times 50\ nm^2$ (Fig. 5c and d), respectively, has been measured. In the beam profile of the MCP image in the x direction, edge enhancement is clearly visible. Edge enhancement occurs when the beam grazes across the slanted vertical side-wall of the grid, which increases the contact area of the beam with the grid significantly. Even for a perfectly straight and smooth side-wall, edge enhancement occurs as secondary electrons are emitted from the beam path as it passes parallel to the edge. Edge enhancement in the y direction is low enough to be 'drowned out' by the step function of direct surface emission. Edge enhancement theoretically is helpful as it increases yield, but becomes a burden if the sidewall is not perfectly straight. A resolution standard with high side-wall verticality is therefore vital for a more accurate determination of beam size using electron detection. Later experiments, in which similar procedures have been carried out using electron detection on a fresh spot on the Ni grid, have resulted in a beam focus of $17 \times 34\ nm^2$, as measured by the MCP, seen in Fig. 5e and f.

4. Outlook and conclusion

We have provided a way to fabricate high quality free standing Ni resolution standards featuring orthogonal, smooth grid bars and a side-wall slope projection of less than 6 nm. This resolution standard is ideal in determining the beam spot size for PBW. This grid can also be used in the field of masked proton lithography [19] and with minor adjustments the fabrication procedure can be used to fabricate multi-level molds and stamps. The beam characterization through the MCP detector can further be improved by optimizing the positioning and biasing of the MCP detector, thereby increasing the detector's yield. These experiments would help in increasing the image resolution and decreasing acquisition time.

An orthogonal free-standing grid with high side wall verticality has been made using improved fabrication techniques. The high degree of orthogonality enables focusing in the x- and y-direction independently. The newly fabricated grid has been used successful in the process of focusing a 2 MeV H_2^+ beam. Owing to the high

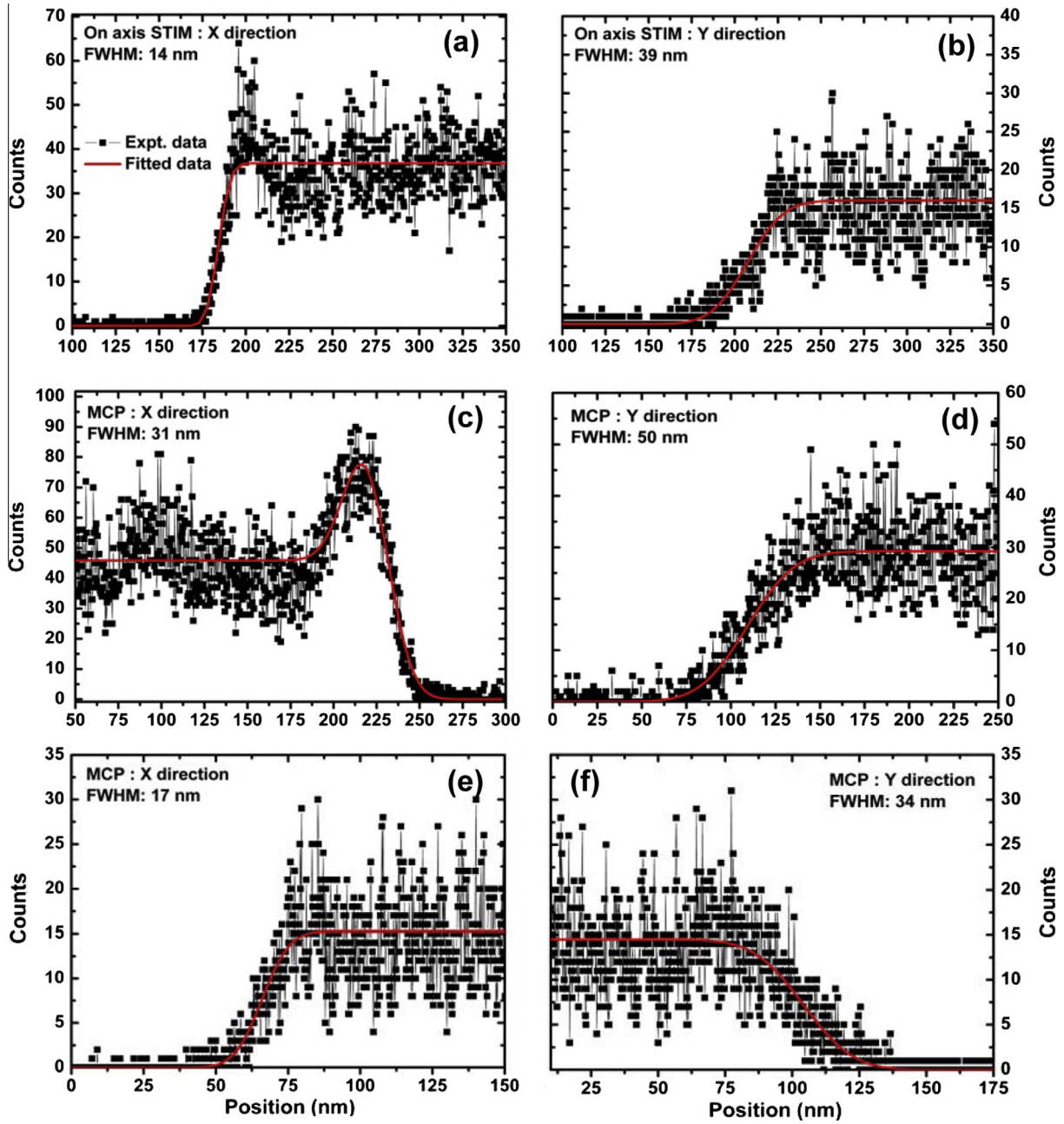

Fig. 5. Beam profiles using (a and b) on-axis STIM, and (c and d) ion induced secondary electron detection by MCP. The beam profiles in (a)–(d) were scanned over edges of the grid from the region as shown with a white marker line in Fig. 4a and c. Later, using similar procedures on a fresh spot on the Ni grid, the beam profiles in (e) and (f) have been acquired with MCP, showing a beam spot size of 17 × 34 nm^2.

current densities the PIN diode suffers damage and its performance degrades within a short time span. Electron detection (using MCP detector) is an attractive alternative to surpass this shortcoming. In initial experiments a beam spot size down to 14 and 17 nm have been obtained with on-axis STIM and electron imaging respectively. These exercises demonstrate that easy and direct beam focusing is possible with MCP detector at typical currents used during PBW experiments.

Acknowledgments

The authors acknowledge the financial support rendered by A-Star, Singapore (R-144-000-261-305) and US Air Force and MOE T1 (R-144-000-265-112).

References

[1] F. Watt, A.A. Bettiol, J.A. van Kan, E.J. Teo, M.B.H. Breese, Int. J. Nanosci. 4 (2005) 269–286.
[2] J.A. van Kan, A.A. Bettiol, F. Watt, Appl. Phys. Lett. 83 (2003) 1629–1631.
[3] J.A. van Kan, A.A. Bettiol, F. Watt, Nano Lett. 6 (2006) 579–582.
[4] R. Rajendran, M.Q. Ren, M.D. Ynsa, Biochem. Biophys. Res. Commun. 382 (2009) 91–95.
[5] J.A. van Kan, P.G. Shao, P. Molter, M. Saumer, A.A. Bettiol, T. Osipowicz, F. Watt, Nucl. Instrum. Methods Phys. Res. Sect. B 231 (2005) 170–175.
[6] F. Zhang, J.A. van Kan, S.Y. Chiam, F. Watt, Nucl. Instrum. Methods Phys. Res. Sect. B 260 (2007) 474–478.
[7] F. Watt, M.B.H. Breese, A.A. Bettiol, J.A. van Kan, Mater. Today 10 (2007) 20–29.
[8] J.A. van Kan, P. Malar, A. Baysic de Vera, Xiao Chen, A.A. Bettiol, F. Watt, Nucl. Instrum. Methods Phys. Res. Sect. A 645 (2011) 113–115.
[9] J.A. van Kan, P. Malar, A. Baysic de Vera, Rev. Sci. Instrum. 83 (2012). 02B902-1–02B902-3.
[10] E.J. Teo, M.B.H. Breese, A.A. Bettiol, F. Watt, J. Vac. Sci. Technol. A 22 (2004) 560–564.

[11] R. Minqin, J.A. van Kan, A.A. Bettiol, L. Daina, C.Y. Gek, B.B. Huat, H.J. Whitlow, T. Osipowicz, F. Watt, Nucl. Instrum. Methods Phys. Res. Sect. B 260 (2007) 124–129.
[12] K. Ansari, J.A. van Kan, A.A. Bettiol, F. Watt, Appl. Phys. Lett. 85 (2004) 476–478.
[13] J.F. Ziegler, J.P. Biersack, U. Littmark, The Stopping and Range of Ions in Solids, Pergamon, New York, 1985, Chapter 8. Available from: <http://www.srim.org>.
[14] M. Köhler, Etching in Microsystem Technology, Wiley-VCH, Weinheim, Germany, 1999. pp. 4.
[15] G. Dearnaley, Rep. Prog. Phys. 32 (1969) 405–491.
[16] J.L. Wiza, Nucl. Instrum. Methods 162 (1979) 587–601.
[17] J.A. van Kan, A.A. Bettiol, F. Watt, Mater. Res. Soc. Symp. Proc. 777 (2003) T2.1.1–T2.1.10.
[18] C.N.B. Udalagama, A.A. Bettiol, J.A. van Kan, E.J. Teo, M.B.H. Breese, T. Osipowicz, F. Watt, Nucl. Instrum. Methods Phys. Res. Sect. B 231 (2005) 389–393.
[19] I. Adesida, Nucl. Instrum. Methods Phys. Res. Sect. B 7–8 (1985) 923–928.